



Article

2D-QSAR and CoMFA Models for Antitubercular Activity of Scalarane-Type Sesterterpenes

Suriyan Thengyai ¹, Yuewei Guo ², Khanit Suwanborirux ³, Heinz Berner ⁴, Helmut Spreitzer ⁴, Peter Wolschann ⁵ , Supa Hannongbua ⁶ and Anuchit Plubrukarn ^{1,*} 

¹ Department of Pharmacognosy and Pharmaceutical Botany, Faculty of Pharmaceutical Sciences, Prince of Songkla University, Songkhla 90112, Thailand

² Department of Natural Products Chemistry, Shanghai Institute of Materia Medica, Chinese Academy of Sciences, Zu Ching Zhu Road, Shanghai 201203, China

³ Department of Pharmacognosy and Pharmaceutical Botany, Faculty of Pharmaceutical Sciences, Chulalongkorn University, Bangkok 10330, Thailand

⁴ Department of Drug and Natural Product Synthesis, Althanstrasse 14, Universitat Wien, 1090 Wien, Austria

⁵ Institute of Pharmaceutical Technology and Biopharmacy, Althanstrasse 14, Universitat Wien, 1090 Wien, Austria

⁶ Department of Chemistry, Faculty of Science, Kasetsart University, Bangkok 10900, Thailand

* Correspondence: anuchit.pl@psu.ac.th

Abstract: A series of scalarane sesterterpenes were prepared using heteronemin (**1**) as a primary precursor. Combined with the scalarane derivatives obtained from natural sources, a total of 22 antitubercular scalaranes were used to build QSAR models based in the 2D-QSAR and CoMFA approaches. Both models indicated the influences of substitutions in the vicinity of C-12 and C-16 of the scalaranes. A 2D-QSAR model suggested the necessity of hydrophilic functionalities on the peripherals with hydrophobic cores, and the lowering steric repulsion to improve the potential energy. This was complemented by the pictorial CoMFA model, which indicated the importance of the positive electrostatic with shortened steric extension crowning over C-12 and the lengthy negative functionalities extended from C-16.

Keywords: structure-activity relationship; sesterterpenes; tuberculosis; marine natural products



Citation: Thengyai, S.; Guo, Y.; Suwanborirux, K.; Berner, H.; Spreitzer, H.; Wolschann, P.; Hannongbua, S.; Plubrukarn, A. 2D-QSAR and CoMFA Models for Antitubercular Activity of Scalarane-Type Sesterterpenes. *Sci. Pharm.* **2022**, *90*, 47. <https://doi.org/10.3390/scipharm90030047>

Academic Editors: Roman B. Lesyk and William A. Donaldson

Received: 9 June 2022

Accepted: 9 August 2022

Published: 15 August 2022

Publisher's Note: MDPI stays neutral with regard to jurisdictional claims in published maps and institutional affiliations.



Copyright: © 2022 by the authors. Licensee MDPI, Basel, Switzerland. This article is an open access article distributed under the terms and conditions of the Creative Commons Attribution (CC BY) license (<https://creativecommons.org/licenses/by/4.0/>).

1. Introduction

Tuberculosis is among the neglected diseases that place a heavy burden on the developing world. The disease was declared a global public health emergency by the World Health Organization (WHO) in 1993, and enormous efforts have been made to prevent its spread. Such efforts have led to the fall in the incidence rate over the past ten years; yet, apart from the COVID-19 pandemic, tuberculosis is among the top ten causes of death and the leading cause of death due to a single causative pathogen, even higher than HIV/AIDS. In a 2021 report, the WHO estimated the 2020 global tuberculosis incidence to be as staggeringly high as 9.87 million or 127 cases per 100,000 population, with a mortality (HIV-positive and -negative combined) of 1.49 million [1].

One of the most problematic aspects of tuberculosis for disease management is the lengthy treatment period that can last as long as six months. An abrupt stop in taking the antitubercular medicines, especially in economically challenged patients, primarily contributes to the prevalence of multidrug-resistant mycobacterium strains. With a limited choice of first-line drugs for effective treatment, and the less effective second-line drugs with undesirable adverse effects, the need for new antitubercular medicines, preferably with new modes of action, has hastened the search for leads that may offer an alternative in tuberculosis treatment for health care providers.

From our search for drug leads from Thai marine bioresources, we reported the antitubercular activity of marine-derived scalarane sesterterpenes isolated from the sponge of

the genus *Hyrtilios* (formerly identified as *Brachiaster* sp.) [2,3]. The representative analog heteronemin (**1**) was first isolated from the sponge *Heteronema erecta* [4,5], and later from several other sources, including the sponges of the genera *Hyatella* and *Hyrtilios*, and from the nudibranch *Glossodoris atromarginata* [6–11]. The antitubercular activity of **1** was first recognized by El Sayed et al. [12]. However, the compound has not been considered an attractive antitubercular drug candidate due to its potent and indiscriminating cytotoxicity [7,12]. In our previous report, we noticed that certain derivatives, namely compounds **2** and **3**, showed promising selectivity towards antitubercular activity (MICs 3 and 4 μM , respectively), but virtually no cytotoxicity against any cancer cell lines described therein [2].

Preliminary QSAR and CoMFA (Comparative Molecular Field Analysis) models based on 14 natural and chemically-derived scalaranes (compounds **1–14**) had been conducted [13]. The results suggested that the antitubercular activity of the scalaranes could potentially be influenced by the oxygenated functionalities surrounding the furan moiety of the pentacyclic skeleton of the scalaranes. However, as most of the compounds that constituted the dataset during our preliminary study were natural products, the structural variation was rather serendipitous and random. In this study we expanded the dataset, comprising both the newly derived compounds and natural scalaranes, for more refined models. Referred to in our preliminary results, the primary foci for the chemical derivatizations are a modification towards the electrostatic and non-static fields crowning C-12 and the negative electrostatic and lengthy extension from C-16. The results from the devised models are compared, and possible SARs for the antitubercular activity of the scalaranes are described.

2. Materials and Methods

2.1. General Procedures

Unless stated otherwise, solvents and chemicals were all reagent grade and were used as purchased without further purifications. Chromatographic solvents were commercial grade and were redistilled prior to use. For the chemical reactions, THF was distilled over benzophenone/sodium and used immediately, and CH_2Cl_2 was distilled over CaH_2 onto 4 Å molecular sieve. All chemical reactions were performed under dried argon atmosphere in oven-dried vessels.

The UV spectra were obtained from a Shimadzu UV-160A (Markham, ON, Canada), and IR spectra were from Perkin Elmer Spectrum One FT-IR spectrometers (Shelton, CT, USA), both in the operating solvents or matrixes indicated accordingly. All of the NMR experiments were performed either on a Varian Unity Inova 500 (Palo Alto, CA, USA), or on a Bruker Avance 500 spectrometer (Billerica, MA, USA) (both at 500 MHz for ^1H). The chemical shifts referred to those of the operating solvents as described accordingly. EI mass spectra were obtained from an MAT 95 XL mass spectrometer (Waltham, MA, USA).

2.2. Chemical Derivatizations

Heteronemin (**1**) was used as the primary starting material for the syntheses of compounds **15–28** and their preceding intermediates (**4,9,10,13**). The starting material was isolated from the sponge *Hyrtilios* sp. as described previously [2,3], and was imported to this investigation with no additional purification. The synthesized compounds were identified using the complete spectroscopic analyses. The spectroscopic data of **13** and **15–28** are compiled in Supplementary Materials.

Scalarafuran (13) and 16-Deacetoxyscalarafuran (15). To an ice-cold solution of iodine (115 mg, 0.45 mmol) and triphenylphosphine (124 mg, 0.47 mmol) in CH_2Cl_2 (5 mL), a solution of **1** (150 mg, 0.31 mmol) in CH_2Cl_2 (5 mL) in one portion was added. The mixture was stirred for 30 min (0 °C), at which time 5% NaHSO_3 (20 mL) was added, and the mixture was extracted with CH_2Cl_2 (3 \times 20 mL). Chromatography over SiO_2 (petroleum ether/EtOAc 95:5 m then 90:10) afforded **13** (57 mg, 48%) and **15** (40 mg, 29%).

Scalarafuran acetate (16) and 16-Deacetoxyscalarafuran acetate (17). Acetylation of **13** and **15** was performed in the same manner. Each starting material (**13**; 10 mg, 0.023 mmol;

and **15**; 10 mg, 0.024 mmol) was stirred with Ac₂O (1 mL, 11 mmol) in CH₂Cl₂ (5 mL) for 20 h, and saturated NaHCO₃ (10 mL) was added. After an extraction in CH₂Cl₂ (3 × 20 mL), each mixture was chromatographed over SiO₂ (petroleum ether/EtOAc 9:1 for **16**; petroleum ether/EtOAc 97.5:2.5 for **17**) to yield **16** and **17** (10 mg, 91%; and 10 mg, 89%, respectively).

12-Oxoscalarafuran (18) and 12,16-Deacetoxy-12-oxoscalarafuran (19). PCC oxidation was performed on **13** (74 mg, 0.17 mmol) and **15** (20 mg, 0.054 mmol). PCC (110 mg, 0.51 mmol for **13**; 25 mg, 0.12 mmol for **15**), coated on an appropriate amount of SiO₂, was stirred in 10 mL CH₂Cl₂. To each suspension was added either a solution of **13** or **15** in CH₂Cl₂, and the mixture was stirred for 4 h, then filtered through a celite pad and washed with EtOAc (3 × 10 mL). Each combined filtrate was diluted with CH₂Cl₂, washed with water (2 × 10 mL), and chromatographed over SiO₂ (petroleum ether/EtOAc 95:5 for **18**; petroleum ether/EtOAc 97.5:2.5 mg for **19**) to yield **18** and **19** (58 mg, 82%; and 14 mg, 70%, respectively).

12-E-Oximinoscalarafuran (20) and 12, 16-Deacetyl-12-E-oximinoscalarafuran (21). Oximation was performed on **18** (15 mg, 0.035 mmol) and **19** (14 mg, 0.038 mmol). Each oxo starting material was refluxed with NH₂OH.HCl (12 mg, 0.17 mmol for **18**, and 8 mg, 0.12 mmol for **19**) and NaOAc (14 mg, 0.17 mmol, each) in EtOH (5 mL each) for 2 h. Once cooled, the solvent was removed, and each mixture was chromatographed over a SiO₂ column (petroleum ether/EtOAc 9:1 for both **20** and **21**) to yield **20** and **21** (16 mg, 96%; and 13 mg, 89%, respectively).

12-E-O-Methyloximinoscalarafuran (22) and 12,16-Deacetoxy-12-E-O-methyloximinoscalarafuran (23). Oximation toward the methoxyoximes was performed on **18** and **19** in the same manner as described for the preparation of **20** and **21**. Oxos **18** (15 mg, 0.035 mmol) and **19** (14 mg, 0.038 mmol) were each refluxed with NH₂OMe.HCl (5 mg, 0.06 mmol for **18**, and 7 mg, 0.083 mmol for **19**) and NaOAc (7 mg, 0.085 mmol, each) in EtOH (10 mL, each) for 2 h. Upon solvent removal, each mixture was chromatographed over SiO₂ (petroleum ether/EtOAc 9:1 for **22**; petroleum ether/EtOAc 95:5 for **23**) to yield **22** and **23** (10 mg, 60%; and 13 mg, 58%, respectively).

Sesterstatin (24). To a solution of **13** (15 mg, 0.035 mmol) in 1:1 CH₂Cl₂/THF (4 mL), 50% KOH (10 mL) was added. The resulting suspension was refluxed for 2 h, at which time saturated NH₄Cl (10 mL) was added. The mixture was extracted with CH₂Cl₂ (2 × 10 mL) and chromatographed over a SiO₂ column (petroleum ether/EtOAc 7:3) to afford **17** (12 mg, 89%).

12-Deacetyl-12-epi-scalaradiol (25). To a solution of **1** (50 mg, 0.10 mmol) in MeOH, 10 mL) NaBH₄ (38 mg, 1 mmol) was added. The mixture was stirred at room temperature for 3 h. AcOH (1 mL) and water (10 mL) were added, and the mixture was extracted with CH₂Cl₂ (3 × 10 mL). The dried extract was chromatographed over a SiO₂ column (CHCl₃/MeOH 95:5) to yield **25** (31 mg, 80%).

12-O-Deacetyl-16 α -nitromethyl-16 β ,17 α -dihydro-19-deoxyscalarin (26) and 12-O-Deacetyl-16 α -nitromethyl-16 β ,17 α -dihydro-19-deoxyscalarin (27). To a solution of **25** (20 mg, 0.05 mmol) in CH₂Cl₂ (7 mL), MnO₂ (87 mg, 1 mmol) was added. The suspension was stirred at room temperature for 2 h. The resulting mixture was filtered through a celite pad and washed with EtOAc (3 × 10 mL). The crude residue was separated over a SiO₂ column (petroleum ether/EtOAc 8:2) to yield **4** (14 mg, 72%).

A 2-mL solution of **4** (11 mg, 0.028 mmol) in CH₂Cl₂ was added to CH₃NO₂ (57 mg, 0.93 mmol) and DBU (51 mg, 0.34 mmol) in CH₂Cl₂ (3 mL). The mixture was stirred at room temperature for 20 h, at which time saturated NH₄Cl (10 mL) was added. After subsequent extraction with CH₂Cl₂ (2 × 10 mL), the extract was chromatographed over a SiO₂ column (petroleum ether/EtOAc 7:3), and **26** and **27** were obtained (4.5 mg, 36%; and 5 mg, 39%, respectively).

16-Deacetoxyscalarapyridazine (28). To a stirred solution of **1** (20 mg, 0.041 mmol) in MeOH (10 mL), NaHCO₃ (22 mg, 0.26 mmol) was added. The mixture was stirred at room temperature for 5 h. After removing the solvent, the crude residue was chromatographed

over a SiO₂ column (petroleum ether/EtOAc 7:3) to yield **9** and **10** as an inseparable mixture, which was used without any further purification. The solution of **9** and **10** in CH₂Cl₂/EtOH (1:1, 5 mL) was stirred with N₂H₄·H₂O (2.4 mL, 0.05 mmol) at room temperature for 1 h. After an extraction with CH₂Cl₂ (2 × 10 mL), and chromatography over a SiO₂ column (EtOAc/MeOH 93:7), **28** (8 mg, 54% after 2 steps) was obtained.

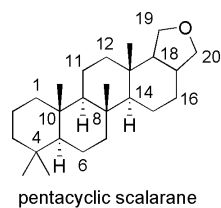
2.3. Antitubercular Activity

All compounds to be incorporated in the compound dataset, except for **6–10**, which were no longer available at the time of this investigation, were subjected to the antitubercular activity determination using a green fluorescent protein-based technique [14]. The bioassay was serviced by the Central Bioassay Laboratory, National Center of Genetic Engineering and Biotechnology (BIOTEC), Pathumthani, Thailand. The targeted microbe was green-fluorescent-protein-expressing *M. tuberculosis* H37Ra (ATCC25177). The inhibition percentage was calculated based on the fluorescent intensities of treated-over-untreated cultures and reported in MIC. The activity was referred to those of rifampicin, streptomycin, isoniazid, and ofloxacin as standard drugs. For the unavailable compounds **6–10**, the antitubercular activities were referred to the previously reported MICs obtained from the microplate alamar blue assay [15].

2.4. Compound Dataset

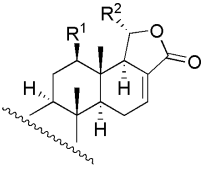
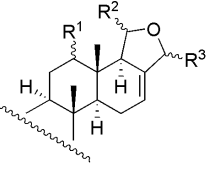
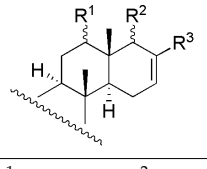
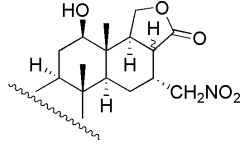
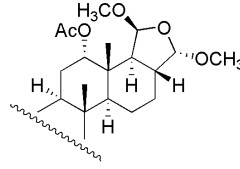
The compound dataset comprised 33 scalarane sesterterpene derivatives (Table 1). In addition to 14 newly modified analogs described in 2.2 (compounds **15–28**), included were 19 compounds (compounds **1–14**, **29–33**) that have previously been reported by us. Among these 19 compounds, 11 were natural products, isolated from the sponge *Hyrtilis* sp. (compounds **1–2**, **4–7**) [2,3] and from the nudibranch *Grossodoris rufomarginata* (compounds **29–33**) [16]. Compounds **3** and **8–14** were chemically derivatized from heteronemin (**1**), and were readily identified in our previous studies [3]. The previously reported compounds that were subjected to the green fluorescent assay (**1–5**, **11–14**, **29–33**) were transferred to this investigation with no additional purification. The integrity of the imported compounds was confirmed on the basis of the NMR spectroscopy.

Table 1. Scalarane derivatives in compound dataset.



Compounds	MIC (μM) ^a			Compounds	MIC (μM) ^a				
	obs.	calc.			obs.	calc.			
		2D-QSAR	CoMFA			2S-QSAR	CoMFA		
1	R ¹ = -OH; R ² = α - OAC	3	1.6	3.4	13	R ¹ = -OH; R ² = -OAC	14	16.2	11.2
2	R ¹ = -OAc; R ² = α - OAC	3	1.6	1.8	14	R ¹ = -OH; Δ ¹⁵	135	104.7	128.8
3	R ¹ = =O; R ² = α - OAC	0.2	0.6	0.4	15 ^c	R ¹ = -OH; R ² = -H	270	-	-
29 ^b	R ¹ = -OAc; R ² = β - OAC	12	5.5	13.1	16 ^c	R ¹ = -OAc; R ² = -OAC	NA	-	-

Table 1. Cont.

Compounds	MIC (μM) ^a			Compounds	MIC (μM) ^a			
	obs.	calc.			obs.	calc.		
		2D-QSAR	CoMFA			2S-QSAR	CoMFA	
				17 ^c	$\text{R}^1 = -\text{OAc}; \text{R}^2 = -\text{H}$	970	-	-
				24	$\text{R}^1 = -\text{OH}; \text{R}^2 = -\text{OH}$	65	66.1	87.1
	4	$\text{R}^1 = -\text{OH}; \text{R}^2 = -\text{H}$	16	34.7	22.4			
5	$\text{R}^1 = -\text{OAc}; \text{R}^2 = -\text{H}$	117	63.1	83.2				
6	$\text{R}^1 = -\text{H}; \text{R}^2 = -\text{OAc}$	4	15.8	3.6				
				18 ^c	$\text{X} = \text{O}; \text{R} = -\text{OAc}$	235	-	-
				19 ^c	$\text{X} = \text{O}; \text{R} = -\text{H}$	272	-	-
				20	$\text{X} = \text{E} - \text{NOH}; \text{R} = -\text{OAc}$	28	30.9	33.9
				21	$\text{X} = \text{E} - \text{NOH}; \text{R} = -\text{H}$	65	57.5	53.7
				22	$\text{X} = \text{E} - \text{NOCH}_3; \text{R} = -\text{OAc}$	110	151.4	97.7
				23 ^b	$\text{X} = \text{E} - \text{NOCH}_3; \text{R} = -\text{H}$	126	228.1	266.0
	7	$\text{R}^1 = \beta - \text{OH}; \text{R}^2 = \alpha - \text{OAc}; \text{R}^3 = \beta - \text{OCH}_3$	54	46.8	46.8			
8	$\text{R}^1 = \beta - \text{OH}; \text{R}^2 = \alpha - \text{OH}; \text{R}^3 = -\text{H}$	257	446.7	182.0				
30	$\text{R}^1 = \beta - \text{OH}; \text{R}^2 = \beta - \text{OCH}_3; \text{R}^3 = \alpha - \text{OCH}_3$	56	72.4	64.6				
31 ^c	$\text{R}^1 = \alpha - \text{OAc}; \text{R}^2 = \beta - \text{OCH}_3; \text{R}^3 = \alpha - \text{OCH}_3$	NA	-	-				
				26	$\beta - \text{H} - 17$	28	13.8	38.9
				27	$\alpha - \text{H} - 17$	28	50.1	26.3
	9	$\text{R}^1 = \beta - \text{OH}; \text{R}^2 = \beta - \text{CHO}; \text{R}^3 = -\text{CHO}$	65	41.7	52.5			
10	$\text{R}^1 = \beta - \text{OH}; \text{R}^2 = \alpha - \text{CHO}; \text{R}^3 = -\text{CHO}$	8	13.5	6.8				
11	$\text{R}^1 = =\text{O}; \text{R}^2 = \beta - \text{CHO}; \text{R}^3 = -\text{CHO}$	130	45.7	120.2				
12	$\text{R}^1 = \beta - \text{OAc}; \text{R}^2 = \beta - \text{CHO}; \text{R}^3 = -\text{CHO}$	58	57.7	104.7				
25 ^c	$\text{R}^1 = \beta - \text{OH}; \text{R}^2 = \beta - \text{CH}_2\text{OH}; \text{R}^3 = -\text{CH}_2\text{OH}$	NA	-	-				
33 ^c	$\text{R}^1 = \alpha - \text{OAc}; \text{R}^2 = \beta - \text{CHO}; \text{R}^3 = -\text{CHO}$	NA	-	-				
				28		263	263.0	295.1
				32 ^c		210	-	-

Note: obs. = observed MIC; calc. = calculated MIC; NA = not active at the highest concentration tested. ^a All of the calculations for the QSAR models were performed in pMIC scale. ^b Test set. ^c These compounds were not included to the dataset either because they were not active (NA) at the highest concentration of 400 $\mu\text{g}/\text{mL}$, therefore unavailable MICs, or the low solubility did not permit the precise MICs to be obtained.

2.5. QSAR

The 2D-QSAR and CoMFA approaches for the QSAR studies were carried out using the antitubercular activities, calculated as pMICs, of 22 compounds from the compound dataset as a training set (see Section 3.3 below). For the 2D-QSAR, the geometrical optimization was performed on Gaussian03 (Wallingford, CT, USA) and the descriptor calculation was computed using Molecular Operating Environment (MOE2008) (Montreal, QC, Canada). In the CoMFA approach, the studies were conducted on SYBYL 7.0 (St. Louis, MO, USA), courtesy of the National Electronics and Computer Technology Center (NECTEC), Bangkok. Data analysis for QSAR evaluation was performed on SPSS 1.2.

2.5.1. 2D-QSAR Model

In the 2D-QSAR setting, the 3D structures of compounds in the training and test sets were energetically refined with a density function theory of B3LYP under a 6–31 g (d, p) basis set. The calculation of 327 physico-chemical properties of each compound was performed in the lowest-energy, optimized conformations. The relevant particular physico-chemical properties resulted from said calculation were selected using a stepwise method.

2.5.2. CoMFA Model

For the CoMFA model, each molecule was optimized to yield the lowest-energy conformation under the Tripos Force Field, and the partial charge was calculated on each atom based on the Gasteiger-Huckel charge calculation. The alignments, based on fit atom, matching, and superimposition, were performed on the obtained conformations by fixing C-1 to C-10 of compound **3** as a template. The grid box was automatically created to cover all aligned molecules with a 4-Å extension in all directions. The interactions, namely electrostatic and steric, were computed between all grid points located at each intersection of box defined by sp^3 carbon with charge +1 and atoms of molecules. Electrostatic and steric parameters were collected from those probe atoms to evaluate the model.

The molecular field data was treated with PLS to correlate with the antitubercular activity. The coefficient of determination, F ratio, and SEE were used to evaluate the quality of the model. The leave-one-out experiment was carried out to determine the predictability of the resulting models.

3. Results and Discussion

The main objective of this investigation is to establish improved 2D-QSAR and CoMFA models for the antitubercular activity of the scalaranes using a rebuilt larger compound dataset. In addition to 14 compounds previously described in our preliminary runs [13], included in this dataset are 14 new semi-synthetic derivatives and five additional natural scalaranes, comprising a total of 33 scalarane analogs.

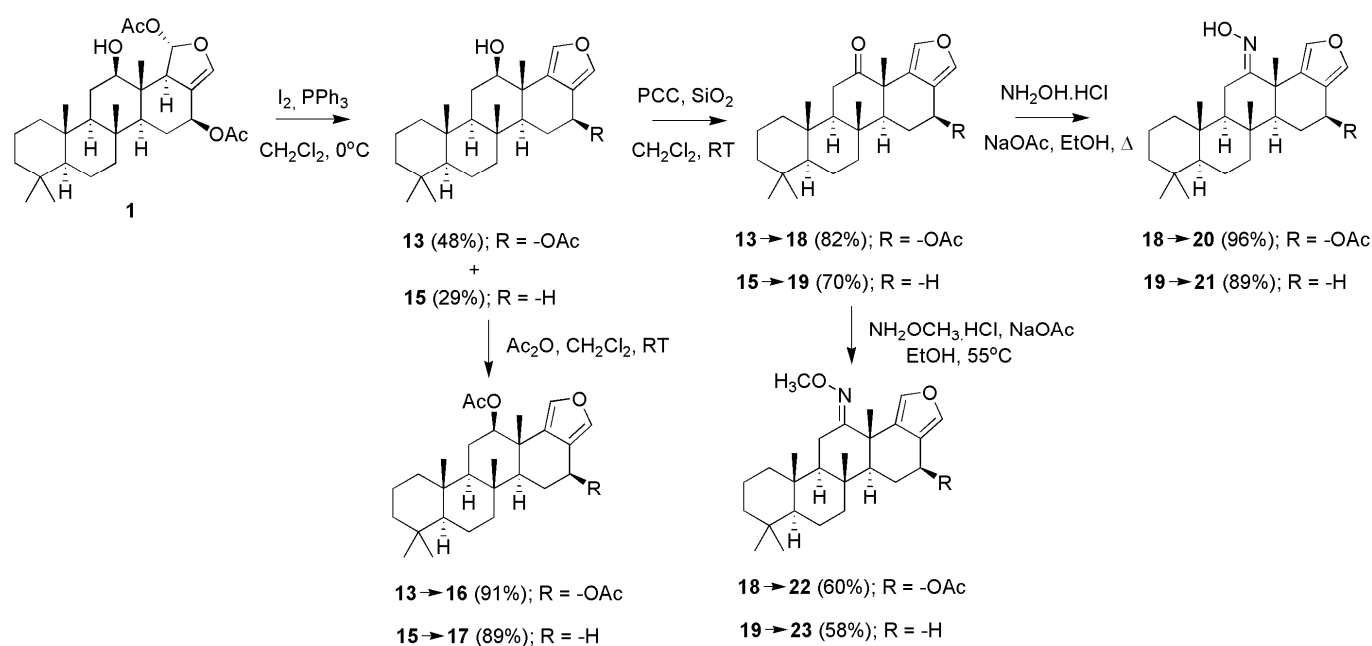
3.1. Derivatization of the Scalaranes

As described earlier, the main foci of the chemical derivatization performed in this study is the specific manipulation of the electrostatic field surrounding C-12, C-16, and C-19, as suggested by our preliminary results [13]. A total of 18 scalaranes were prepared in this investigation using heteronemin (**1**) as the primary starting material. Among 18 synthesized compounds, four (compounds **4**, **9**, **10**, and **13**) were readily available as natural products [2,3], and were described in this part of the investigation solely as intermediates for the further derivatization. In addition, compounds **15** and **24** were also reported previously as natural products, whereas **16–23** and **25–28**, a total of 12 compounds, were newly synthesized and reported here for the first time.

3.1.1. Scalarafuran Series

Deacetoxylation of **1** using triphenylphosphine-iodine [17,18] led to **13** and **15** as two major products (Scheme 1). Both compounds were previously reported as natural products [3,19,20], and were used here primarily as intermediates for the further manipulation

on the oxygenated functionalities on C-12. Note that although our previous results suggested that the furan moiety may lower the potency at least one magnitude (for example, **1** vs. **13**), therefore making it not entirely beneficial for antitubercular activity [13], the furan ring offered a stability better than did its furanol and furanone counterparts. This superior stability allowed the chemical transformation, particularly on the oxygenated functional groups on C-12 and C-16, to be conducted. The side reaction towards dideacetylated **15** was unexpected, and its mechanisms have never been documented nor described. However, incorporating **15** and the subsequent derivatives to the dataset shall demonstrate the importance of substituting groups on C-16 (or the lack thereof; see Section 3.1.2) to the antitubercular activity.

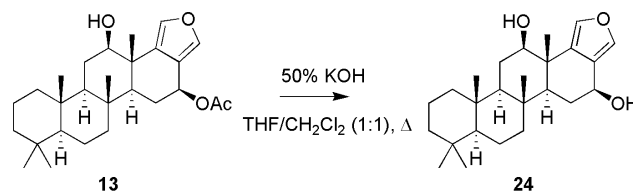


Scheme 1. Preparation of compounds in scalarafuran series.

The modifications of 12-OH of **13** and **15** performed here included acetylation (**16** & **17**), oxidation (**18** & **19**), and coupling with methoxylamine and hydroxylamine (**20–23**) [21] (Scheme 1). The structural variation allowed a good range of electrostatic functionalities over C-12.

The geometry of the oximes **20–23**, presumably governed by the repulsion from the nearby furan ring, was deduced to be *E*. This is supported by the chemical shift differences of α carbons on both sides of the oxime, as compared between the oxo starting materials and resulting oximes ($\Delta\delta_{\text{C}\alpha} = \delta_{\text{C}\alpha\text{-oxo}} - \delta_{\text{C}\alpha\text{-oxime}}$; Table S1, Supplementary Materials) [22,23]. The proposed geometry contradicted the results from the NOE-DS experiments in which the dipolar couplings between H-19s and methoxy protons of **22** and **23** were observed. However, the calculations indicated that the inter-atomic distances between H-19 and the methoxy protons on either *E* or *Z* geometries of both derivatives were in an indistinguishable range for the NOE (Figures S69 and S70, Supplementary Materials). In fact, the steric repulsion in the *Z* conformers led to farther inter-atomic distances for both **22** and **23**. The results from $\Delta\delta_{\text{C}\alpha}$ s, on the other hand, provided more concrete evidence that indicated the *E* geometry unambiguously. The approach can also be used with compounds **20** and **21**, the exchangeable protons of which were unobservable, hence were inapplicable NOE experiments. Therefore, the determination of the oxime geometry based on the chemical shift differences prevailed.

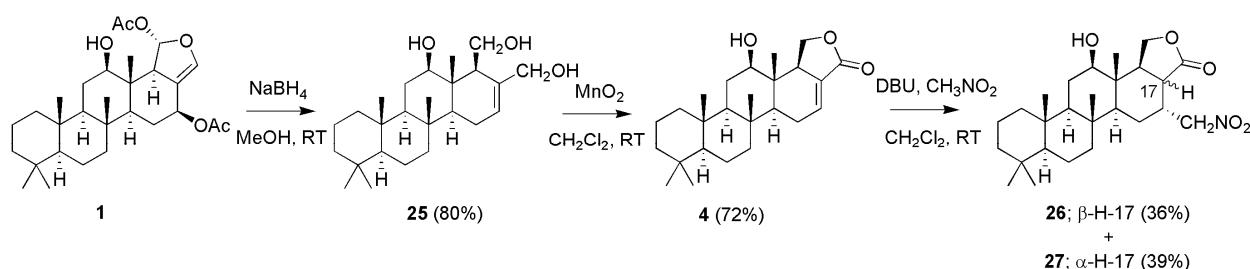
A hydrolysis of **13** yielded a 16-deacetyl derivative **24** (Scheme 2). The compound is identical to sesterstatin, a natural sesterterpene previously isolated from *Hyrtios erecta* sponge [24]. The presence of the hydroxy group on C-16 of **24** added the electrostatic variation on the C-16 extension of the scalarafuran series.



Scheme 2. Deacetylation of **13** towards **24**.

3.1.2. Deoxyscalarin Series

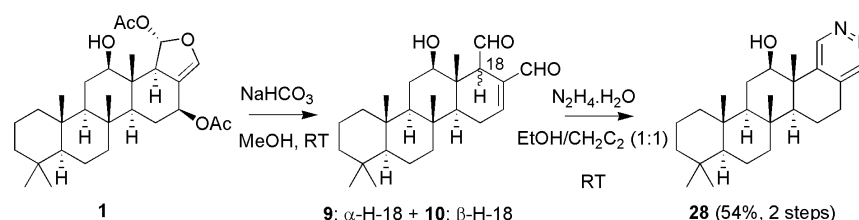
In addition to the oxygenated functionalities on C-16, the alkyl extensions on this side of the scalarane skeleton were attempted. Reduction of **1** with a borohydride led to a spontaneous ring opening toward the triol **25** (Scheme 3). An oxidation with Mn(IV) [25] recycled the resulting intermediate allylic aldehyde toward the furanone **4**, which was subjected to a β -alkylation with nitromethane to yield epimeric nitromethyls **26** and **27** [26]. Disappointingly, alkylation on C-16 of **4** with various alkyl cuprates failed to yield any C-16 alkyl-substituted analogs.



Scheme 3. Preparation of compounds in deoxyscalarin series.

3.1.3. Scalaradials and Scalarapyridazine

The acetoxy acetal moiety of **1** proved to be too labile for the extensive deacetylation. When a similar hydrolysis condition described for **13** toward **24** was applied to **1**, the results failed to yield any isolatable products. Even with a mild methanolysis, the resulting hemiacetal spontaneously underwent a ring opening and yielded a mixture of diols **9** and **10** [10]. The mixture, although available in a limited amount, was used to prepare the pyridazine **28** [27] (Scheme 4), adding to the aromatic variation other than the furans and dihydrofurans.



Scheme 4. Preparation of **28**.

3.2. Determination of Antitubercular Activity

Fourteen chemically derived scalaranes (**15–28**) and five natural sesterterpenes (**29–33**) were subjected to an antitubercular activity determination using a green fluorescent assay protocol targeting *M. tuberculosis* H37Ra (ATCC25177) [14]. Due to the different assay protocol from our first report [2,3,13,15], compounds from the previous dataset (**1–5**,

11–14), except for 6–10 which were no longer available, were re-examined with the green fluorescent assay. For the compounds that were not re-tested, the activities were referred to the previous reports [3,13] with an assumption that the two bioassays acceptably provided the comparable results [14]. The activities of the compounds in the dataset are shown in Table 1.

3.3. Structure Activity Relationship and Computer Modeling

Upon obtaining the newly derived and natural scalaranes, all compounds, including those from the previous report, were considered for integrating into the QSAR analyses. Compounds 23 and 29 were arbitrarily selected to be in the test set due to the relevant functionalities on C-12 and C-16 amended according to our preliminary results [13], therefore allowing a predictability assessment. The compounds that were inactive (16, 25, 31, 33) were automatically dismissed. In addition, due to the incomplete solubility of 15, 17, 18, 19, and 32, hence inaccurate MICs, these compounds were also excluded. A total of 22 compounds were imported to the new training set. The MICs of the compounds in the dataset spanned from 0.23 (pMIC 6.67) to 263 μM (pMIC 3.58) (pMIC range 3.09, \bar{x} 4.53 \pm 0.74, s^2 0.55, for 22 compounds).

3.3.1. 2D-QSAR

Geometric optimization of each compound for the 2D-QSAR was performed at an ab initio level (B3LYP) and with a 6–31 g (d, p) basis set (Gaussian03). The resulting optimized conformation was used to calculate 327 physico-chemical descriptors (MOE2008). Based on a step-wise selection (SPSS12), four descriptors emerged to yield the best fitting Equation (1). (See Table S2, Supplementary Materials for the calculated values of each molecular descriptor.)

$$\text{pMIC} = 8.860(\pm 0.881) - 0.057(\pm 0.010)E_{\text{nb}} - 2.168(\pm 0.304)vsurf_{\text{ID2}} + 2.976(\pm 0.642)vsurf_{\text{CW3}} - 0.021(\pm 0.004)PEOE_{\text{VSA}+1} \quad (1)$$

where

$E_{\text{nb}} \rightarrow = \rightarrow$ potential energy with all bonded terms disabled,

$vsurf_{\text{ID2}} \rightarrow = \rightarrow$ hydrophobic integrity moment,

$vsurf_{\text{CW3}} \rightarrow = \rightarrow$ capacity factor, and

$PEOE_{\text{VSA}+1} \rightarrow = \rightarrow$ sum of v_i (van der Waals surface area of atom i); for an atom i , where q_i is a partial charge of such atom i , and is in the range of [0.05,0.10), expressed as

$$dq_{ij} = \frac{1}{2^k} \frac{(x_i - x_j)}{x_j^+}$$

The coefficient for each descriptor is expressed as a mean(\pm SD).

The resulting model gave an acceptable linearity ($r^2 = 0.878$), Figure 1, dash line) and predictability ($q^2 = 0.774$). Based on the resulting SAR (Equation (1)), the calculated MICs agreed well with the observed data, showing residual MICs deviating in a range smaller than 25 μM (Figure 2). The exception was the activities of compounds 5, 8 and 11, the calculated MICs of which deviated larger than 50 μM . The weak correlations among the four descriptors based on 22 compounds in the dataset (Table 2) suggested the independence of each descriptor from one another.

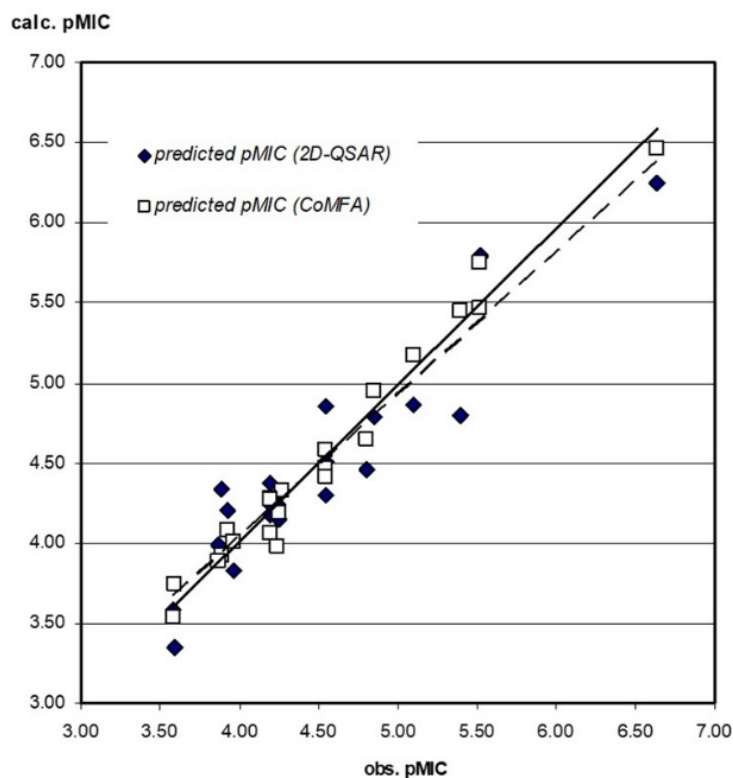


Figure 1. Correlations between the observed and calculated pMICs based on the 2 D-QSAR (dash line; expressed as $y = 0.884 x + 0.5066$, $r^2 = 0.878$) and CoMFA (solid line; expressed as $y = 0.9729 x + 0.1226$, $r^2 = 0.973$) models (both $p = 0.000$).

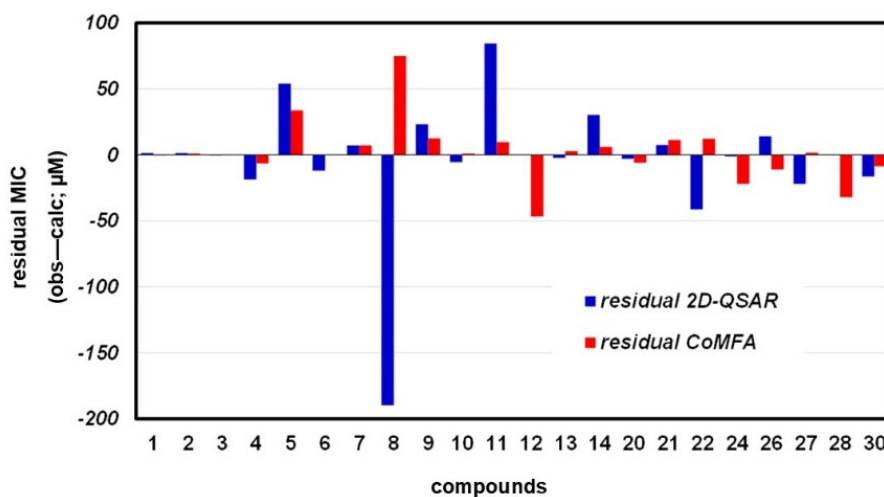


Figure 2. Residual MICs (observed–calculated) for compounds subjected to QSAR analyses.

Table 2. Pearson’s correlation matrix of working descriptors.

	E_{nb}	$vsurf_{ID2}$	$vsurf_{CW3}$	$PEOE_{VSA+1}$
E_{nb}	1			
$vsurf_{ID2}$	−0.2354	1		
$vsurf_{CW3}$	−0.2885	0.6236	1	
$PEOE_{VSA+1}$	0.4329	−0.6096	−0.3434	1

With a larger array of calculated descriptors provided by MOE, the re-established model offered a better fitted QSAR function. This was indicated by q^2 , which improved from 0.685 [13] in the preliminary results to 0.774, shown above. Due to the different software (Material Studio vs. MOE), all of the four descriptors involved here differed entirely from those predicted in our preliminary runs [13]; however, related properties were inherited. For example, both volume-surface descriptors ($vsurf_{ID2}$ and $vsurf_{CW3}$) were closely related to the dipole moments, with direct implications for the steric influences. Complementing each other, $vsurfs$ indicated the improved potency by means of spreading out the hydrophilic functionalities onto the peripheral surface of the molecules, and holding the hydrophobicity closely and tightly to the inner cores of the structures. For E_{nb} , in addition to a direct interpretation that the more stable the compound, the better the activity, the functions that were calculated with disabled bonded terms implied that such stability may be achieved through less steric repulsion among each substituent. The last descriptor, $PEOE_{vsa+1}$, in fact reflected the influences of $RPCG$ (ratio of positive charge of the most positive atom over the total positive charge) previously employed [13]. $PEOE_{vsa+1}$ indicated the influence of charge at a single atom level, but rather integrating more of the polarizing factors through van der Waals surface areas than the ionic characters formerly implied by $RPCG$.

3.3.2. CoMFA Model

Parallel with the 2D-QSAR approach, the CoMFA study was carried out. Three alignment rules were trialed (see Section 2.5.2). The computational parameter was best met when employing the superimposition alignment rule, with sp^3 C as the probing atoms. This agreed well with the methods attempted in the previous report [13].

The CoMFA results (Figure 3) concurred with the prediction in the previous study [13] and allowed a parallel interpretation. This included the negative electrostatic and steric disfavored regions (blue and yellow patches, respectively) that hovered over C-12, and indicated the need for positive dipole moment inducers with as little bulkiness as possible, e.g., an oxo functionality in **3**. On the other end, the negative electrostatic and steric favored regions (red and green patches, respectively) extending from C-16 reflected the positive influences of an acetoxy group substituted at this position.

The re-established CoMFA models yielded much improved linearity from that obtained from the 2D-QSAR model ($r^2 = 0.973$, Figure 1, solid line). However, the predictability, despite being in an acceptable range with a q^2 of 0.630, was lower than that provided by the 2D-QSAR model described above, and that of the CoMFA calculation using the smaller dataset (q^2 0.810) [13]. This may be attributed to compounds with larger and more flexible substitutions being added to the new dataset. Compared with the results from the 2D-QSAR, despite less predictability, the better alignment between the observed and calculated MICs (Table 1) was demonstrated here as there was only one compound (**8**) that showed a residual MIC larger than 50 μ M (Figure 2).

The ratio between the electrostatic and steric contributions in the resulting CoMFA model was 59:41. The contribution ratio that was in favor of the electrostatic influences sounded controversial, as the antitubercular drug leads should rather be hydrophobic for they have to penetrate through the mycolic acid-coated cell wall of the mycobacterium. That is, a higher proportion from the steric contribution, hence hydrophobic implication, shall be expected. A closer look into the compound dataset, however, suggested that the compounds in the dataset differed mainly in their electrostatic substitutions. These electrostatic functionalities dominated the model and reflected in the resulting contribution ratio. Nonetheless, if $\log P$ of each compound (average 5.69, range 4.53–7.06; see Supplementary Materials), albeit not integrated directly into any QSAR functions, was considered, the range of strong hydrophobicity indeed agreed well with such a requirement.

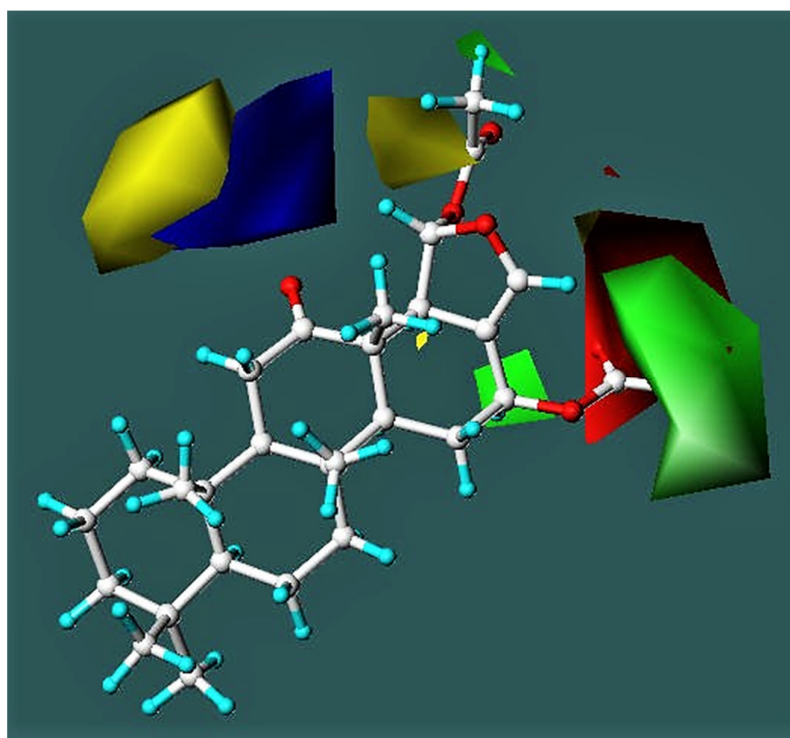


Figure 3. Contour plot of potential pharmacophoric functionalities calculated from the CoMFA QSAR model, based on the structure of **3**. Color code is as follows: blue = positive-electrostatic favored regions, red = positive-electrostatic disfavored regions, green = steric favored regions, yellow = steric disfavored region.

3.3.3. Compound Test Set

Compounds **23** and **29** were subjected to the calculation as the test set (Table 1). The calculated MICs of **29** based on both models were in a good agreement with the observed activity. Notice that **29** is in fact a 19-epimer of **2**. The slightly lower potency of **29** than that of **2** provides a good evidence of the predicted negative effects from the steric field in the vicinity of C-12, particularly on the β plane.

As for **23**, although its calculated and observed pMICs were in the same magnitude (observed pMIC 3.90; calculated pMICs based on 2D-QSAR 3.64, on CoMFA 3.58), the calculated MICs of **23** from both models strayed from the one observed by more than 50 μ M. This in part resulted from the disadvantage of the assay protocol, in which two-fold dilution was performed to obtain MICs, therefore leading to the wider and less precise gaps between consecutive dilutions as the concentration become larger. Nevertheless, combined with the results from **5**, **8**, and **11**, all of which also showed inaccuracy in either, or both, predictions, it is noticeable that all have no C-16 extensions. Such inaccuracy indicated that the derived models may underestimate the influences from such extensions, and the effects from the functionalities both on C-12 and on C-16 may need to be more comprehensively integrated.

Considering the compounds that were dismissed from the dataset as inactive analogs (compounds **16**, **25**, **31**, and **33**), both resulting QSAR models sufficiently reflected the lack in the activity and merited such dismissal. To a certain extent, a similar comparison may also extend to accommodate the compounds that were excluded due to low solubility (compounds **15**, **17–19**, and **32**); i.e., most could be predicted to be weakly active to virtually inactive. The arguable case was **18**, which possessed two beneficial functionalities, a 12-oxo and a 16-OAc. The compound, however, was marginally active (observed MIC 235 μ M). Unfortunately, **18** was no longer available at the time of the QSAR analysis. A confirmative determination on its activity was unable to be performed, and such a controversial argument remains unsolved.

4. Conclusions

In summary, a series of scalaranes, both natural and chemically derived, were assessed for the QSARs of the antitubercular activity based on the 2D-QSAR and CoMFA approaches. Yielding acceptable linearity and predictability, the models complemented and agreed well with each other. Despite lower q^2 , the pictorial CoMFA method yielded less deviated calculation. Both models showed that the areas crowning C-12 and the extended regions from C-16 of the scalarane skeleton effectively influenced the potency. In addition, although not being integrated directly, the hydrophobicity reflected by $\log P$ indirectly plays an important role for the active analogs, crucial for the active compounds to penetrate through the lipophilic cell wall of the mycobacteria.

Based on the observed and calculated results, **3**, which was the most active, fit best as a prospective platform for the further modification and investigation. The finding may open up an opportunity to extend the search for new chemical entities for the antitubercular drugs. Our results may also facilitate the search for new drug targets and binding sites for the antitubercular and other related activities.

Supplementary Materials: The following supporting information can be downloaded at: <https://www.mdpi.com/article/10.3390/scipharm90030047/s1>; Spectral data of compounds **13**, **15–28**, Figures S1–S68: IR, NMR, and mass spectra of compounds **1**, **13**, **15–18**, Figures S69 and S70: Calculated interatomic distances between H-19 and 12-NOCH₃ for *E* and *Z* configuration of **22** and **23**, respectively, Table S1: $\Delta\delta_{C\alpha}$ of compounds **20–23**, Table S2: Calculated working molecular descriptors of scalaranes in the compound dataset.

Author Contributions: Methodology, investigation, and data curation, S.T.; resources, Y.G., H.B., H.S., P.W. and S.H.; supervision, H.B., H.S., S.H. and A.P.; project administration, P.W., K.S. and A.P.; conceptualization, writing, and editing, A.P.; funding acquisition, Y.G., K.S. and A.P. All authors have read and agreed to the published version of the manuscript.

Funding: This research was funded by the Higher Education Research Promotion and National Research University Project of Thailand (PHA540439S), Office of the Higher Education Commission, Thailand, and by Prince of Songkla University Research Supporting Grants (PHA530056S and PHA 590351S). S.T. thanks the Royal Golden Jubilee PhD Program (5.G.PS/48/H.1), and the Thailand Research Fund for his thesis supporting grants. The Chinese-Thai collaboration was partially funded by the Sino-Thai Bilateral project of NFSC (no. 2091140471).

Acknowledgments: An appreciation is extended to NECTEC, Thailand, for the access to SYBYL software. We thank the late B. Hodgson, Faculty of Pharmaceutical Sciences, Prince of Songkla University, for his editorial and scientific comment on the primary draft of this article.

Conflicts of Interest: The authors declare that they have no conflict of interest.

References

1. World Health Organization. *Global Tuberculosis Report 2021*; World Health Organization: Geneva, Switzerland, 2021; pp. 4–10.
2. Wonganuchitmeta, S.; Yuenyongsawad, S.; Keawpradub, N.; Plubrukarn, A. Antitubercular sesterterpenes from the Thai sponge *Brachiaster* sp. *J. Nat. Prod.* **2004**, *67*, 1767–1770. [[CrossRef](#)] [[PubMed](#)]
3. Jaisamut, S.; Thengyai, S.; Yuenyongsawad, S.; Karalai, C.; Plubrukarn, A.; Suwanborirux, K. Structure-activity relationships of antitubercular scalaranes: Heteronemin revisited. *Pure Appl. Chem.* **2009**, *81*, 1019–1026. [[CrossRef](#)]
4. Kazlauskas, R.; Murphy, P.T.; Quinn, R.J.; Wells, R.J. Heteronemin, a new scalarin type sesterterpene from the sponge *Heteronema erecta*. *Tetrahedron Lett.* **1976**, *17*, 2631–2634. [[CrossRef](#)]
5. Yashman, Y.; Rudi, A. The ¹³C-NMR spectrum and stereochemistry of heteronemin. *Tetrahedron* **1977**, *33*, 2997–2998. [[CrossRef](#)]
6. Karuso, P.; Cambie, R.C.; Bowden, B.F.; Bergquist, P.R. Chemistry of sponges, VI. Scalarane sesterterpenes from *Hyatella intestinalis*. *J. Nat. Prod.* **1989**, *52*, 289–293. [[CrossRef](#)]
7. Crews, P.; Bescansa, P. Sesterterpenes from a common marine sponge, *Hyrtios erecta*. *J. Nat. Prod.* **1986**, *49*, 1041–1052. [[CrossRef](#)]
8. Kobayashi, M.; Okamoto, T.; Hayashi, K.; Yokoyama, N.; Sasaki, T.; Kitagawa, I. Marine natural products. XXXII. Absolute configurations of C-4 of the manoalide family, biologically active sesterterpenes from the marine sponge *Hyrtios erecta*. *Chem. Pharm. Bull.* **1994**, *42*, 265–270. [[CrossRef](#)]
9. Ledroit, V.; Debitus, C.; Ausseil, F.; Raux, R.; Menou, J.-L.; Hill, B. Heteronemin as a protein farnesyl transferase inhibitor. *Pharm. Biol.* **2004**, *42*, 454–456. [[CrossRef](#)]

10. Kamel, H.N.; Kim, Y.B.; Rimoldi, J.M.; Fronczek, F.R.; Ferreira, D.; Slattery, M. Scalarane sesterterpenoids: Semisynthesis and biological activity. *J. Nat. Prod.* **2009**, *72*, 1492–1496. [[CrossRef](#)]
11. Fontana, A.; Cavaliere, P.; Ungur, N.; D'Souza, L.; Parameswaram, P.S.; Cimino, G. New scalaranes from the nudibranch *Glossodoris atromarginata* and its sponge prey. *J. Nat. Prod.* **1999**, *62*, 1367–1370. [[CrossRef](#)]
12. El Sayed, K.A.; Bartyzel, P.; Shen, X.; Perry, T.L.; Zjawiony, J.K.; Hamann, M.T. Marine natural products as antituberculosis agents. *Tetrahedron* **2000**, *56*, 949–953. [[CrossRef](#)]
13. Thengyai, S.; Maitarat, P.; Hannongbua, S.; Suwanborirux, K.; Plubrukarn, A. Probing the structural requirements for antitubercular activity of scalarane derivatives: 2D-QSAR and CoMFA approaches. *Monatsh. Chem.* **2009**, *141*, 621–629. [[CrossRef](#)]
14. Changsen, C.; Franzblau, S.G.; Palittapongarnpim, P. Improved green fluorescent protein reporter gene-based microplate screening for antituberculosis compounds by utilizing and acetamidase promoter. *Antimicrob. Agents Chemother.* **2003**, *47*, 3682–3687. [[CrossRef](#)] [[PubMed](#)]
15. Collins, L.A.; Franzblau, S.G. Microplate Alamar blue assay versus BACTEC 460 system for high-throughput screening of compounds against *Mycobacterium tuberculosis* and *Mycobacterium avium*. *Antimicrob. Agents Chemother.* **1997**, *41*, 1004–1009. [[CrossRef](#)] [[PubMed](#)]
16. Gavagnin, M.; Mollo, E.; Docimo, T.; Guo, Y.-W.; Cimino, G. Scalarane metabolites of the nudibranch *Glossodoris rufomarginata* and its dietary sponge from the South China Sea. *J. Nat. Prod.* **2004**, *67*, 2104–2107. [[CrossRef](#)] [[PubMed](#)]
17. Alvarez-Manzaneda, E.J.; Chahboun, R.; Cabrera Torres, E.; Alvarez, E.; Alvarez-Manzaneda, R.; Haidour, A.; Ramos, J. Triphenylphosphine-iodine: An effective reagent for the regioselective dehydration of tertiary alcohols. *Tetrahedron Lett.* **2004**, *45*, 4453–4455. [[CrossRef](#)]
18. Alvarez-Manzaneda, E.J.; Chahboun, R.; Cabrera Torres, E.; Alvarez, E.; Alvarez-Manzaneda, R.; Haidour, A.; Ramos, J. Synthesis of alkenes from tertiary esters utilizing the triphenylphosphine-iodine system. *Tetrahedron Lett.* **2005**, *46*, 1075–1077. [[CrossRef](#)]
19. Doi, Y.; Shigemori, H.; Ishibashi, M.; Mizobe, F.; Kawashia, A.; Nakaike, S.; Kobayashi, J. New sesterterpenes with nerve growth factor synthesis-stimulating activity from the Okinawan marine sponge *Hyrtios* sp. *Chem. Pharm. Bull.* **1993**, *41*, 2190–2191. [[CrossRef](#)]
20. Tsukamoto, S.; Miura, S.; Van Soest, R.W.M.; Ohta, T. Three new cytotoxic sesterterpenes from a marine sponge *Spongia* sp. *J. Nat. Prod.* **2003**, *66*, 438–440. [[CrossRef](#)]
21. Cui, J.-G.; Fan, L.; Huang, L.-L.; Liu, H.-L.; Zhou, A.-M. Synthesis and evaluation of some steroidal oximes as cytotoxic agents: Structure/activity study (I). *Steroids* **2009**, *74*, 62–72. [[CrossRef](#)]
22. Hawkes, G.E.; Herwig, K.; Roberts, J.D. Nuclear magnetic resonance spectroscopy. Use of ¹³C spectra to establish configurations of oximes. *J. Org. Chem.* **1974**, *39*, 1017–1028. [[CrossRef](#)]
23. Bunnell, C.A.; Fuchs, P.L. Rapid and unequivocal determination of syn-anti stereochemistry for toluenesulfonylhydrazones and other imine derivatives via carbon-13 nuclear magnetic resonance spectroscopy. A synthetic adjunct. *J. Org. Chem.* **1977**, *42*, 2614–2617. [[CrossRef](#)]
24. Pettit, G.R.; Cichacz, Z.A.; Tan, R.; Herald, D.L.; Melody, N.; Hoard, M.S.; Doubek, D.L.; Hooper, J.N.A. Antineoplastic agents 385. The isolation and structure of a scalarane-type sesterterpene from the Indian Ocean porifera *Hyrtios erecta*. *Collect. Czech. Chem. Commun.* **1998**, *63*, 1671–1677. [[CrossRef](#)]
25. Furuichi, N.; Hata, T.; Soetjipto, H.; Kato, M.; Katsumura, S. Common synthetic strategy for optically active cyclic terpenoids having a 1,1,5-trimethyl-*trans*-decalin nucleus: Syntheses of (+)-acuminolide, (–)-spongianolide A, and (+)-scalarenial. *Tetrahedron* **2001**, *57*, 8425–8442. [[CrossRef](#)]
26. Rosso, G.B.; Pilli, R.A. Diastereoselective addition of nitro compounds to α,β -unsaturated γ -butyrolactones. *Tetrahedron Lett.* **2006**, *47*, 185–188. [[CrossRef](#)]
27. Ismail, K.A.; El-Tombary, A.A.; AboulWafa, O.M.; Omar, A.M.E.; El-Rewini, S.H. Novel steroidal 1,4-diketones and pyridazine derivatives as potential antiestrogens. *Arch. Pharm. Pharm. Med. Chem.* **1996**, *329*, 433–437. [[CrossRef](#)]